The Potassium Ion Channel: Comparison of Linear Scaling Semiempirical and Molecular Mechanics Representations of the Electrostatic Potential

Andrey A. Bliznyuk,*,† Alistair P. Rendell,‡ Toby W. Allen,§ and Shin-Ho Chung§

Supercomputer Facility, Australian National University, Canberra, ACT 0200, Australia, Department of Computer Science, Australian National University, Canberra, ACT 0200, Australia, and Department of Physics, Australian National University, Canberra, ACT 0200, Australia

Received: August 7, 2001; In Final Form: October 12, 2001

The molecular electrostatic potential inside the potassium channel protein from *Streptomyces lividans* has been investigated using linear scaling semiempirical quantum chemical method, for a variety of geometries, with and without solvating water molecules. The results are compared with those given by a number of popular molecular mechanics force-fields. The difference between the quantum and molecular mechanics electrostatic potentials due to the protein exceeds 30 kcal/mol within the narrow selectivity filter of the channel and is attributed to the neglect of electronic effects, e.g., polarization, in the molecular mechanics force-fields. In particular, mutual electronic interactions between four threonine residues in the selectivity filter are found to have a large effect on the electrostatic potential. Calculations in the presence of water molecules suggest that molecular mechanics methods also overestimate the stabilization of the cation inside the ion channel. The molecular electrostatic potentials computed by molecular mechanics force-fields expressed relative to bulk water, however, reveal a much smaller error.

Introduction

Until recently, the theoretical investigation of molecular systems containing many thousands of atoms was limited to molecular mechanics (MM)[1] based methods. In these schemes, the motions of the electrons are ignored, and the total system energy is given purely as a function of the nuclear positions of the constituent atoms. This is, of course, a very crude approximation, but it is widely used in a number of popular MM force-fields (e.g., Amber,[2] OPLS,[3] and Charmm[4]), and for many problems, it gives results that are in good agreement with experiment.[1,5]

Not surprisingly, MM methods fail when the process under study is accompanied by large changes in the electronic distribution. Obvious examples of this are bond-breaking and bond-forming reactions. For this important class of problems, one way to address this limitation is to divide the global system into regions—typically, a small region that is treated using quantum mechanics (QM) and "the rest" treated using MM. The aim of these so-called QM/MM methods is to quarantine electronic changes within the domain of the QM atoms, where the coordinates of each electron are considered explicitly and large changes in the electronic distribution can, at least in principle, be described correctly. Even though QM/MM methods have enjoyed some success,[6] most of these procedures still assume a static charge distribution for the MM region and do not permit transfer of charge from the QM to the MM region. Thus, there remains the fundamental question of how important are electronic effects, such as polarization and charge transfer, in large systems.

The recent development of linear-scaling QM methods,[7] particularly for semiempirical QM methods,[8−11] now enables QM calculations to be performed on systems with thousands of atoms. While such methods are still substantially more expensive than MM methods, they do permit limited QM calculations on systems that traditionally would only have been studied using MM methods. As a consequence, it is now possible to make quantitative assessments of the importance of electronic effects in large systems. This work is an attempt to do this, comparing the electrostatic potential obtained from a variety of MM force-fields with that given by the AM1 semiempirical QM method. This comparison is particularly pertinent, given that the Amber,[2] OPLS,[3] and Charmm[4] MM methods used here and the AM1 [12] semiempirical QM method were all parametrized to reproduce the electrostatic potential obtained from 6-31G* ab initio Hartree−Fock calculations, albeit the electrostatic potential for simple isolated molecules.

The system that we have chosen to study is the KcsA potassium channel protein from *Streptomyces lividans*.[13] Potassium channels that exist in all biological organisms are central to neuronal signaling, as they govern the transfer of K^+ ions through cell membranes.[14] As with all ion channels, understanding the basic mechanism of ion permeation and selectivity is of great interest, and as a result, such systems have received considerable theoretical attention.[15] This is especially true for the KcsA potassium channel since the publication of its X-ray structure in 1998.[13] This channel selectively conducts K^+ ions with high throughput (10 pA[16]) while suppressing conduction of the chemically very similar Na^+ ion by a factor of approximately 10^4. In an attempt to understand ion permeation through this system at a microscopic level, several molecular dynamics studies have been performed previously.[17−22] The work presented here is based on selective structures taken from our previous MD simulations.[17]

* Corresponding author. Phone: 61-2-6125-8924. Fax: 61-2-6125-8199. Email: Andrey.Bliznyuk@anu.edu.au.
† Supercomputer Facility.
‡ Department of Computer Science.
§ Department of Physics.

10.1021/jp013069h CCC: $20.00
Published on Web 11/15/2001

A comparison of the potential profiles derived from QM and MM methods for a charged particle moving across the confined geometry is of particular interest, since there is no explicit bond breaking or forming reactions take place as the ion moves across the channel. Moreover, an accurate description of the electrostatic potential at the center of the ion channel and its response to the passing ion are likely to be key ingredients in developing a full understanding of how this complicated biological channel works. Here we address the first of these issues, comparing the QM and MM electrostatic potentials within the channel. In future work, we will consider, at a QM level, the effect of the ion on the surrounding channel.

Method

The coordinates for our calculations were obtained from MD trajectories generated using Charmm v.25 code,[23] as described in ref 17. The channel is oriented in such a way that the *z*-axis coincides with the center of the pore.[17] Two groups of coordinates have been used. In the first group, coordinates were taken from MD simulations on the solvated ion channel, but all water molecules were removed before evaluating the molecular electrostatic potential (MEP) along the central *z*-axis. In the second group, a K^+ ion had been added to the MD simulations and constrained to lie at various locations along the *z*-axis. For this group, the K^+ ion was removed and the MEP evaluated at the location of the missing K^+ nucleus, in the presence of water molecules.

The majority of the MD simulations upon which this work is based[17] were performed using the united atom Charmm19 force-field.[24] This was justified on the basis of comparisons with the all atom Charmm22 force-field[4] and merited because the significant reduction in associated computer time enabled much longer overall simulation times.[17] Use of a united atom force-field to obtain our sample coordinate sets does, however, necessitated the addition of hydrogens before it is possible to perform all atom MM or QM calculations. This was done, where necessary, using appropriate bond lengths and angles. The resulting "all atom" ion channel with water molecules included has 6550 atoms (5920 atoms without water) and typically required about 12 h to converge a single self-consistent-field AM1 calculation using a 400 MHz Sun E3500 workstation. By contrast, to compute a single MD step requires approximately 1 s. Although several different sets of coordinates were extracted from each MD trajectory, for simplicity, only the results from a single set of coordinates are presented here; the other results were analyzed and found to be quantitatively similar. The QM calculations were performed using the Mopac2000 v.1.1 [25] program and the parametrized molecular electrostatic potential method therein.[12] The QM results were compared with the MEP computed using partial atomic charges taken from the Amber,[2] OPLS,[3] Charmm19,[24] and Charmm22[4] force-fields.

Results and Discussions

A schematic representation of the structure of the potassium channel equilibrated with water is shown in Figure 1. The channel is a tetramer of peptide chains. Each of the four subunits consists of 158 amino acid residues of which the positions of 97 were determined by X-ray diffraction.[13] As detailed in ref 17, our model system comprises the entire experimentally determined protein structure and associated terminating groups, giving a total of 396 residues. Also shown in Figure 1 is an outline of the channel's radius profile derived from the experimental coordinates, in the absence of water, and accounting for atomic size. The channel can be seen to extend for

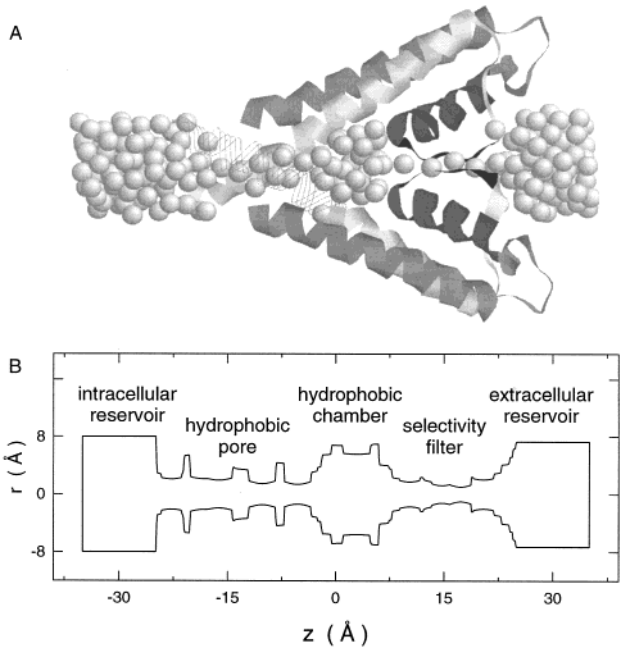

Figure 1. Model of the potassium channel. (A) Two subunits of the KcsA protein are drawn as ribbons while water molecules are drawn as spheres. The inner, outer, and pore helices of the protein are drawn as white, light gray, and dark gray helices, respectively, while the selectivity filter is drawn as a think black ribbon. A section of the inner helix has been replaced by strands to reveal the water molecules (white spheres) within the pore. (B) A trace of the pore radius, based on atomic van der Waals radii, about the channel axis is shown.

approximately 50 Å. While the selectivity filter ($z = 8-22$ Å) is the narrowest region with a mean radius of just 1.4 Å, at one point, the long thin hydrophobic pore ($z = -20$ to -2 Å) also has a minimum radius of just 1.5 Å. Note that these values correspond to the X-ray structure, while the minimum pore radius in the region $z = -20$ to -2 Å obtained from our MD calculations including water[17] exceeds 2 Å. There is experimental evidence that demonstrates that the crystallographic structure may correspond to a "closed"-conduction state.[26] During gating of the KcsA channel, the intracellular pore ($z = -20$ to -2 Å) is thought to widen, reducing the repulsive energy barrier presented to ions. Thus, it is likely that the system under consideration is in a closed state and that MEP contributions from the trans-membrane helices forming the intracellular pore will be affected. On the basis of the proximity of the protein to the *z*-axis, we might expect the MEP in the narrow regions of the channel to show the greatest sensitivity to the means by which it is evaluated. Of particular interest is the MEP near the selectivity filter which remains narrow during gating, and the composition of which is thought to be highly conserved among the potassium channel family.[14]

The MEPs computed along the *z*-axis for a typical coordinate set after removal of water molecules, using three different MM point charges and the AM1 semiempirical QM method, are presented in Figure 2. All MEPs have similar structure with a strong minimum in the region of the selectivity filter ($z = -10$ to 20 Å). This corresponds roughly to the experimentally determined position of two Rb^+ ions.[13] However, it would be incorrect to assign undue significance to this observation since our MEP calculations neglect the presence of both the Rb^+ ions and water molecules in the ion channel.

In line with expectations, the largest differences are in the region of the hydrophobic pore and selectivity filter. First, in the hydrophobic pore ($z = -23$ to -12 Å), the MEP from

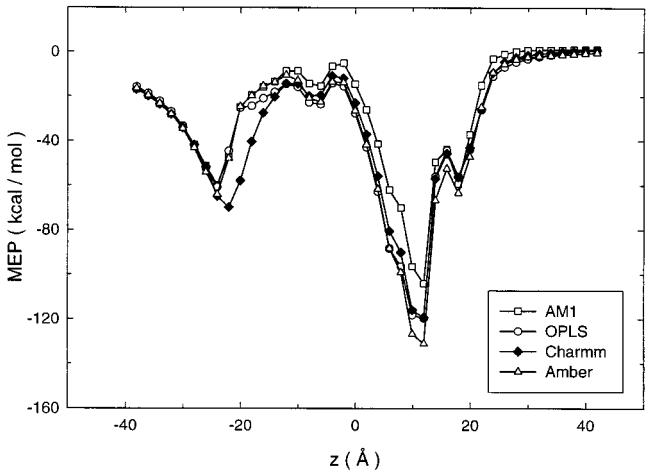

Figure 2. Molecular electrostatic potential inside the protein channel computed using Amber94, Charmm19, OPLS, and AM1 are plotted, as described in the legend. The electrostatic potential for the Charmm22 force-field is not drawn because it is almost identical to the Amber curve.

Charmm19 differs substantially from that of Amber, OPLS, and MOPAC. Second, in a region extending from the hydrophobic chamber to the middle of the selectivity filter ($z = -10$ to 20 Å), there are significant differences between all three MM methods and the QM result. Outside these regions, all four methods agree reasonably well.

Analysis of the MEP on a residue-by-residue basis reveals that the first difference, namely, the difference between Charmm19 and the other MM methods, is due to the use of a united atom representation in the Charmm19 force-field. Specifically, in the region $z = -23$ to -12 Å, one of the four uncharged glutamate (GLU 118) residues is located very close to the *z*-axis. The parameters for this residue, in the neutral form, were taken from ref 27. This treats the −COOH group as a −COO group and places a relatively large negative charge on each of the O atoms (−0.6 e) and counter balancing positive charge (1.35 e) on the C atom. In contrast, Amber and OPLS retain the H atom, assign it a positive charge, and place a negative charge on the attached O atom. For Amber and OPLS, the carboxyl H atom is closest to the *z*-axis giving an overall positive contribution to the MEP. For Charmm19, however, this H atom does not exist, and instead, the MEP is dominated by the associated O atom, giving an overall contribution to the MEP that is negative. While this difference between the united atom Charmm19 and the Amber and OPLS force-fields exists for all glutamates in our system, the much greater distance of these other glutamates from the point of measure of the MEP means that the effect of this difference is far less. Since MOPAC has explicit inclusion of all H atoms, the QM MEP in this region is in much closer agreement to that of either Amber or OPLS than it is to that of Charmm19. Finally, we note that the discrepancy between Charmm19 and other MM force-fields may have been amplified by the very narrow pore associated with the closed state of the channel under consideration. Also, if the all-atom Charmm22[4] force-field is used, the MEP is nearly identical to that of Amber.

As we will now show, the differences between all three force-fields and the QM results in the hydrophobic chamber and early part of the selectivity filter arises from electronic effects that are only included in the QM calculations. In this region, the MEP computed using the AM1 method is systematically smaller than those obtained from any of the three different MM force-fields. This is especially noticeable for *z*-coordinates of 0−12 Å, where the difference between the QM and MM potentials exceeds 20 kcal/mol. The largest deviation, of more than 30 kcal/mol, was obtained for the MM potential computed using Amber94[2] point charges. In this region, the largest contribution to the MEP comes from the four threonine 75 residues, belonging to the four subunits forming the selectivity filter. The geometry of these residues is schematically shown in Figure 3. Note that while the KcsA channel consists of a tetramer of four identical peptide chains, at any given step of a molecular dynamics simulation, there is a clear absence of 4-fold symmetry.

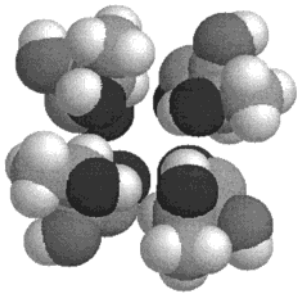

Figure 3. Geometry of the four THR 75 residues. Carbon, oxygen, nitrogen, and hydrogen atoms are drawn as light gray, black, dark gray, and white spheres, respectively.

To verify that the AM1 semiempirical QM method correctly reproduces the MEP obtained from ab initio QM calculations, we added methyl groups to cap both ends of the THR residues and performed ab initio 6-31G* Hartree−Fock calculations using the Gaussian 98 [28] program. The results of these calculations on the four separate THR residues are given in Figure 4A−D. The figure also shows the MEP computed using the Amber force-field[2] i.e., the force field that showed the largest deviation from the QM results.

In general, the results for the isolated THR residues show that both Amber and AM1 reproduce the ab initio MEP very well. The AM1 results have a tendency to underestimate the MEP slightly, while Amber overestimates it slightly, but in all cases, the difference is less than 4 kcal/mol. Similar pictures were obtained using coordinates for these residues taken from several different MD trajectories, suggesting that the influence of the THR geometry on the MEP is relatively small. In contrast, the total MEP computed for a supermolecule comprising all four THR residues shows a marked difference between the QM and MM results. This is shown in Figure 5. The AM1 semiempirical QM method is seen to reproduce the ab initio 6-31G* results very closely, while the Amber point charge results deviate strongly. Comparison of the MEP obtained by summing the MEP from ab initio calculations on the four isolated residues (Figure 4A−D) is also shown in Figure 5. The difference between this and the full supermoleule calculation clearly demonstrates the effect of mutual electronic interactions between the THR residues. Indeed, Mulliken charges computed on the oxygen atoms in the carbonyl groups using the ab initio 6-31G* wave function reduce by approximately 0.5 au when all four residues are present in the supermolecule calculation; an effect that is accounted for by the AM1 calculations but ignored by all the MM force-fields used here.

It should be noted, however, that while the four THR residues account for a substantial fraction of the difference between the MM and QM MEP in the region of the selectivity filter, there are also substantial other electronic effects. To illustrate this point, Figure 6 compares the Amber and AM1 MEPs for the protein when all four THR residues are removed; the difference is smaller than that in Figure 2 but still exceeds 12 kcal/mol.

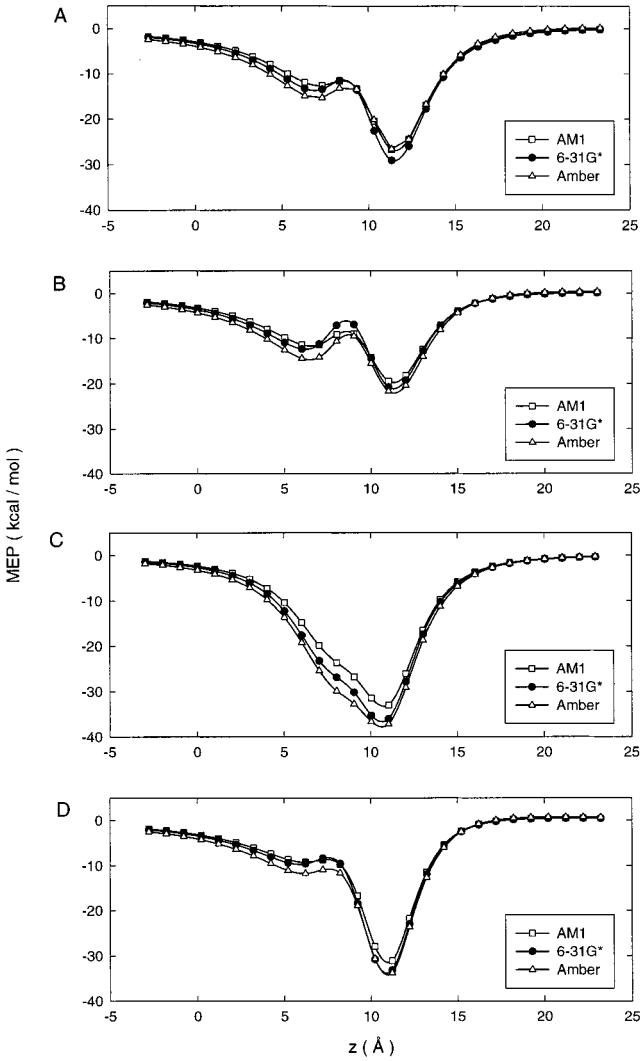

Figure 4. Separate molecular electrostatic potentials along the *z*-axis for the four THR 75 residues are shown in panels A−D. Curves have been computed using ab initio 6-31G*, Amber 94, and AM1 methods, as indicated in the legend.

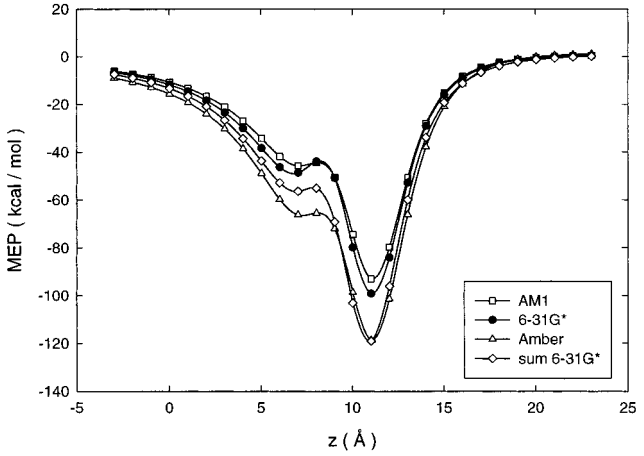

Figure 5. Molecular electrostatic potential computed for all four THR 75 residues together using ab initio 6-31G*, Amber 94, and AM1. The sum of the separate MEP's for the four THR 75 residues computed using ab initio 6-31G* is also shown as a comparison.

Thus far, the MEP has been evaluated in the absence of water. Removal of water permits the MEP to be evaluated at all points along the *z*-axis, since there are no longer any atoms located directly on or very close to this axis. In reality, however, transfer

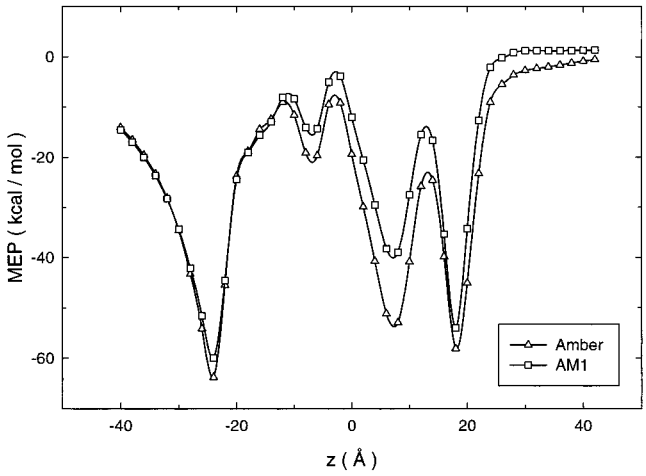

Figure 6. Molecular electrostatic potential of the channel protein, excluding the contribution from the four THR 75 residues for Amber 94 and AM1 methods.

of K^+ ions through the ion channel occurs in the presence of water. To make some assessment of the effect of water on the MEP, we have taken coordinates from simulations in which the K^+ ion was constrained to lie at different *z*-locations, removed the K^+ ion, and evaluated the MEP at the position of the missing K^+ nucleus. In contrast to our previous results, the geometry of the entire ion channel changes between each MEP evaluation. As a consequence, comparison of the MEP between K^+ locations will incur statistical noise. This "noise" may be reduced by sampling many geometries for each K^+ location and averaging the results. Unfortunately, given the expense of the QM calculations, we have only been able to use a small number of geometries (between 2 and 8) at each K^+ location. Thus, our results should only be considered as illustrative, rather than statistically rigorous.

Figure 7 shows the MEP at the various different K^+ locations calculated using the AM1 QM method and point charges taken from the Amber force-field. In panel A the potential arising from the ion channel atoms only is shown, while panel B shows the total MEP. The two curves in Figure 7A are broadly in agreement with the corresponding two curves in Figure 2. In particular, outside the ion channel, the results from the QM and MM calculations agree reasonably well, but around the region of the selectivity filter, the Amber MEP differs from the QM value by about 50 kcal/mol. In the regions outside of the selectivity filter, addition of water (Figure 7B) greatly lowers both the QM and MM MEPs, resulting in an overall flattening of the potential. These large drops in the MEP may be expected given that they occur at points that are now closely surrounded by (solvating) water molecules. What is perhaps more interesting is the observation that the MEP is now fairly constant throughout the entire ion channel. Moreover, it is relatively constant even though the value of the MEP is determined almost entirely by the protein for points within the selectivity filter and by the solvating water molecules at points outside of this region. This feature is common to both the QM and MM calculated MEP.

While the behavior of the MEPs when evaluated using the QM and MM methods appear to be much more similar in the hydrated ion channel compared to analogous calculations on the isolated system, some important differences between the two sets of results exist. Not least is the fact that within the ion channel the MM results are typically 50 kcal/mol more negative than the corresponding QM results, implying a much stronger interaction between the K^+ ion and its surroundings. To highlight the differences between the QM and MM results for

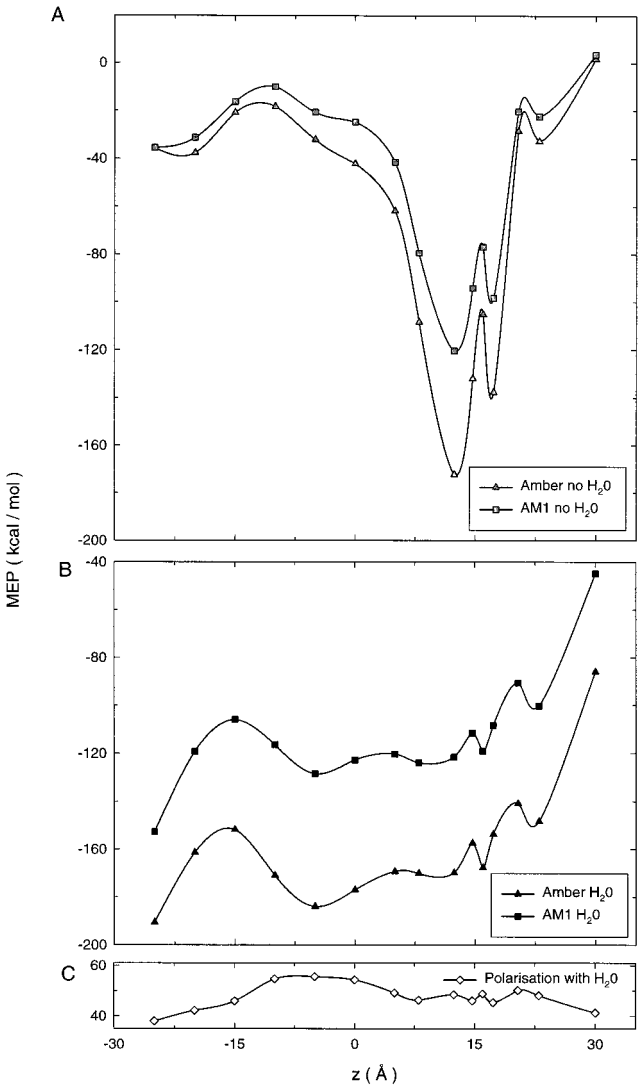

Figure 7. Molecular electrostatic potential computed using Amber94 and AM1 for protein atoms only are shown in panel A, while MEP's for the total system (protein and waters) are shown in panel B. The difference between the AM1 and Amber94 curves in panel B is shown in panel C with the same scale as that used in panels A and B.

the hydrated system, we plot in Figure 7C the difference between the two curves given in Figure 7B corresponding to the solvated systems. This shows that in the ion channel the difference between the QM and MM results is typically around 50 kcal/mol, but fluctuates by about 10 kcal/mol. In the extracellular regions ($z < -25$ and > 30), however, it appears that the difference between the QM and MM results decreases. This implies that in comparison to the QM method, the MM method will more strongly favor a K^+ ion within the ion channel compared to one located outside. To verify this relative behavior, we have again considered how well AM1 and Amber reproduce the MEP from ab initio 6-31G* Hartree−Fock calculations. This time we compare the MEP obtained from the water molecules surrounding the $z = -25$ Å K^+ site. The results of these calculations are shown in Table 1 for three different groups of water molecules; (i) all water molecules within a radius of 15 Å, (ii) all water molecules within a 30 Å radius, and (iii) all water molecules between a radius of 15 and 30 Å.

The data in Table 1 clearly shows that the AM1 method underestimates the MEP for all water shells. This is particularly true for water molecules close to the point of measure of the MEP and may be a reflection of the fact that the AM1 method

TABLE 1: Electrostatic Potential Values in kcal/mol for Different Water Shells about the $z = -25$ Å K^+ Site

	AM1	Amber	ab initio 6-31G*
30 Å shell	−91.4	−122.6	−105.5
15 Å shell	−79.6	−107.8	−89.7
15−30 Å shell	−11.6	−14.8	−13.8

was parametrized to reproduced the ab initio 6-31G* electrostatic potential for water molecules at their optimized AM1 geometry,[12] and not for the SPC/E[29] geometries used here. On the other hand, Amber appears to overestimate the MEP dramatically, especially that associated with nearby water molecules. For MM methods, it may be argued, however, that the van der Waals energy term compensates for this overestimation. This does not appear to be true for our calculations since the van der Waals energies are just 3.4, 5.3, and −1.9 kcal/mol for the 30 Å shell, the 15 Å shell and 15−30 Å shells, respectively. We also note that the van der Waals energies computed for all points given in Figure 7 were found to be only a few kcal/mol. Thus, overall the data in Table 1 suggests that the differences between the QM and MM results for points $z = -25$ and 30 in Figure 7C are likely to be overestimated. This implies that in reality the difference between AM1 and Amber calculations in Figure 7C may in fact be more positive inside the channel with respect to the bulk water. Therefore, even in the presence of water molecules, Amber calculations probably overestimate the stabilization energy of the K^+ ion inside the channel relative to the bulk.

Conclusion

Although the importance of the introducing terms into MM force-field to account for electronic changes (like polarization) is now well recognized,[30−32] the study of such effects has typically been limited to the conformation energies of small molecular systems.[30,32] In contrast, this work has quantitatively compared the results of QM and MM calculations on a large and complex biomolecular system, namely, the potassium ion channel. We have found that large changes in the electronic distributions of individual amino acids in this system are induced by interactions with other nearby amino acids, particularly in the region of the selectivity filter. Failure to account for these effects may lead to substantial errors in the total MEP and, possibly, to errors in the binding energy of a K^+ ion within the ion channel. For a solvated K^+ ion within the pore of the ion channel, however, fluctuations in MEP due to changes in electronic interactions are likely to be much smaller than the absolute error in the MEP. This could explain the considerable success of molecular dynamics simulations of ion channels in finding agreement with experiment. Fixed charge distributions are, however, likely to favor the binding of the K^+ ion within the channel compared to the bulk. Finally, our results indicate that the united atom Charmm19 parameters taken from[28] may not give an accurate representation of the MEP contributions from glutamic acid residues at short distances. This could impact on the energy of an ion entering the potassium channel where glutamic acid side chains line the pore. The results of this study therefore demonstrate that calculations performed with fixed-charge MM force-fields should be viewed with some caution and improved treatments of electronic distributions in ion channels should be sought in the future.

References and Notes

(1) Peterson, I.; Liljefors, T. *Reviews in Computational Chemistry*; VCH Publishes: New York, 1996; Vol. 9, pp 167−189.

(2) Cornell, W. D.; Cieplak, P.; Bayly, C. I.; Gould, I. R.; Merz, K. M., Jr.; Ferguson, D. M.; Spellmeyer, D. C.; Fox, T.; Cadwell, J. W.; Kollman, P. A. *J. Am. Chem. Soc.*, **1995**, *117*, 5179.

(3) Jorgensen, W. L.; Tirado-Rives, J. *J. Am. Chem. Soc.*, **1988**, *110*, 1664.

(4) Mackerell, A. D.; Bashford, D.; Bellott, M.; Dunbrack, R. L.; Evanseck, J. D.; Field, M. J.; Fischer, S.; Gao, J.; Guo, H.; Ha, S.; Josephmccarthy, D.; Kuchnir, L.; Kuczera, K.; Lau, F. T. K.; Mattos, C.; Michnick, S.; Ngo, T.; Nguyen, D. T.; Prodhom, B.; Reiher, W. E.; Roux, B.; Schlenkrich, M.; Smith, J. C.; Stote, R.; Straub, J.; Watanabe, M.; Wiorkiewicz-Kuczera, J.; Yin, D.; Karplus, M. *J. Phys. Chem. B* **1998**, *102*, 3586.

(5) Kollman, P. A.; Massova, I.; Reyes, C.; Kuhn, B.; Huo, S. H.; Chong, L.; Lee, M.; Lee, T.; Duan, Y.; Wang, W.; Donini, O.; Cieplak, P.; Srinivasan, J.; Case, D. A.; Cheatham, T. E. *Acc. Chem. Res.* **2000**, *33*, 889.

(6) Gao, J. *Reviews in Computational Chemistry*; VCH Publishes: New York, 1996; Vol. 7, pp 119−185.

(7) Ordejon, P. *Comput. Mater. Sci.* **1998**, *12*, 157.

(8) Stewart, J. J. P. *Int. J. Quantum Chem.* **1996**, *58*, 133.

(9) Lee, T.; York, D. M.; Yang, W. *J. Chem. Phys.* **1996**, *105*, 2744.

(10) Daniels, A. D.; Milliam, J. M.; Scuseria, G. E. *J. Chem. Phys*. **1997**, *107*, 425.

(11) Dixon, S. L.; Merz, K. M. Jr. *J. Chem. Phys.* **1997,** *107*, 879.

(12) Wang, B.; Ford, G. P. *J. Comput. Chem.* **1993**, *14*, 1101.

(13) Doyle, D. A.; Cabral, J. M.; Pfuetzner, R. A.; Kuo, A.; Gulbis, J. M.; Cohen, S. L.; Chait, B. T.; MacKinnon, R. *Science* **1998**, *280*, 69.

(14) Miller, C. *Genome Biol.* **2000**, *1* 4.

(15) Tieleman, D. P.; Biggin, P. C.; Smith, G. R.; Sansom, M. S. P. *Biochim. Biophys. Acta*, in press.

(16) Schrempf, H.; Schmidt, O.; Kummerlen, R.; Muller, D.; Betzler, M.; Steinkamp, T.; Wagner, R. *EMBO J.* **1995**, *14*, 5170.

(17) Allen, T. W.; Bliznyuk, A.; Rendell, A. P.; Kuyucak, S.; Chung, S.-H. *J. Chem. Phys.* **2000**, *112*, 8191.

(18) Luzhkov, V. B.; Aqvist J. *Biochim. Biophys. Acta* **2000**, *1481*, 360.

(19) Allen, T. W.; Kuyucak, S.; Chung, S.-H. *Biophys. J.* **1999,** *77*, 2502.

(20) Aqvist, J.; Luzhkov, V. *Nature* **2000**, *404*, 881.

(21) Berneche, S.; Roux, B. *Biophys. J.* **2000**, *78*, 2900.

(22) Biggin, P. C.; Smith, G. R.; Shrivastava, I.; Choe, S.; Sansom, M. S. P. *Biochim. Biophys. Acta* **2001**, *1510*, 1.

(23) Brooks B. R., Bruccolerim, R. E.; Olafson, B. D.; States, D. J.; Swaminathan, S.; and Karplus, M. *J. Comput. Chem.* **1983**, *4*, 187.

(24) Neria, E.; Fischer, S.; Karplus, M. *J. Chem. Phys.* **1996**, *105*, 1902.

(25) Stewart, J. J. P. *MOPAC 2000*; Fujitsu Limited: Tokyo, 1999.

(26) Perozo, E.; Cortes, D. M.; Cuello, L. G. *Science* **1999**, *285*, 73.

(27) Lazaridis, T.; Karplus, M. *Proteins* **1999**, *35*, 133.

(28) Frisch, M. J.; Trucks, G. W.; Schlegel, H. B.; Scuseria, G. E.; Robb, M. A.; Cheeseman, J. R.; Zakrzewski, V. G.; Montgomery, J. A., Jr.; Stratmann, R. E.; Burant, J. C.; Dapprich, S.; Millam, J. M.; Daniels, A. D.; Kudin, K. N.; Strain, M. C.; Farkas, O.; Tomasi, J.; Barone, V.; Cossi, M.; Cammi, R.; Mennucci, B.; Pomelli, C.; Adamo, C.; Clifford, S.; Ochterski, J.; Petersson, G. A.; Ayala, P. Y.; Cui, Q.; Morokuma, K.; Malick, D. K.; Rabuck, A. D.; Raghavachari, K.; Foresman, J. B.; Cioslowski, J.; Ortiz, J. V.; Baboul, A. G.; Stefanov, B. B.; Liu, G.; Liashenko, A.; Piskorz, P.; Komaromi, I.; Gomperts, R.; Martin, R. L.; Fox, D. J.; Keith, T.; Al-Laham, M. A.; Peng, C. Y.; Nanayakkara, A.; Gonzalez, C.; Challacombe, M.; Gill, P. M. W.; Johnson, B.; Chen, W.; Wong, M. W.; Andres, J. L.; Gonzalez, C.; Head-Gordon, M.; Replogle, E. S.; Pople, J. A. *Gaussian 98*, Revision A.7; Gaussian, Inc.: Pittsburgh, PA, 1998.

(29) Berendsen, H. J. C.; Grigera, J. R.; Straatsma, T. P. *J. Phys. Chem.* **1987**, *91*, 6269.

(30) Stern, H. A.; Kaminski, G. A.; Banks, J. L.; Zhou, R.; Berne, B. J.; Frieshner, R. A. *J. Phys. Chem. B* **1999**, *103*, 4730.

(31) Winn, P. J.; Ferenczy, G. G.; Reynolds, C. A. *J. Comput. Chem.* **1999**, *20*, 704.

(32) Gane, P. J.; Dean, P. M. *Curr. Opin. Struct. Biol.* **2000**, *10*, 401.